Chinese Physics Letters **40**, 087101 (2023) **Express Letter**

Spectrum of the Hole Excitation in Spin-Orbit Mott Insulator Na_2IrO_3

Wei Wang(王巍)[1], Zhao-Yang Dong(董召阳)[2], Shun-Li Yu(于顺利)[3,4*], and Jian-Xin Li(李建新)[3,4*]

[1]*School of Science, Nanjing University of Posts and Telecommunications, Nanjing 210023, China*
[2]*Department of Applied Physics, Nanjing University of Science and Technology, Nanjing 210094, China*
[3]*National Laboratory of Solid State Microstructures and Department of Physics, Nanjing University, Nanjing 210093, China*
[4]*Collaborative Innovation Center of Advanced Microstructures, Nanjing University, Nanjing 210093, China*

(Received 6 June 2023; accepted manuscript online 3 July 2023)

We study the motion of a hole with internal degrees of freedom, introduced to the zigzag magnetic ground state of Na_2IrO_3, by using the self-consistent Born approximation. We find that the low-, intermediate-, and high-energy spectra are primarily attributed to the singlet, triplet, and quintet hole contributions, respectively. The spectral functions exhibit distinct features such as the electron-like dispersion of low-energy states near the Γ point, the maximum M-point intensity of mid-energy states, and the hole-like dispersion of high-energy states. These features are robust and almost insensitive to the exchange model and Hund's coupling, and are in qualitative agreement with the angular-resolved photoemission spectra observed in Na_2IrO_3. Our results reveal that the interference between internal degrees of freedom in different sublattices plays an important role in inducing the complex dispersions.

DOI: 10.1088/0256-307X/40/8/087101

The charge dynamics of doped Mott insulators have attracted significant attention due to their crucial role in understanding the high-temperature superconducting mechanism in high-T_c cuprates.[1,2] In this regard, the t–J model, featuring antiferromagnetic Heisenberg interactions, is widely considered as an appropriate model for describing the low-energy behavior of doped antiferromagnetic Mott insulator.[3] In such an antiferromagnetically ordered background, the coherent propagation of a single hole at low energies has been theoretically established on the square lattice[1,4–8] and verified by the angle-resolved photoemission spectroscopy (ARPES) experiments.[9]

Recently, much attention has been paid to spin-orbit assisted Mott insulators, where the strong spin-orbit coupling gives rise to a low-energy $J = 1/2$ (multi-electron state) Kramers doublet and a high-energy $J = 3/2$ quadruplet from t_{2g}^5 manifold,[10,11] such as the honeycomb-lattice Na_2IrO_3[12–16] and α-$RuCl_3$.[17–20] The effective $J = 1/2$ spin-orbit entangled states on the honeycomb lattice[15] could induce bond-dependent Kitaev interactions, which can generate a spin-liquid ground state.[21] However, zigzag magnetic ordering[13,18,22,23] has been experimentally observed in these materials at low temperatures, implying the existence of other exchange terms that stabilize the magnetic order. To describe the low-energy magnetic physics, several extended models have been proposed, ranging from nearest-neighbor Heisenberg terms[15,24,25] and off-diagonal Γ interaction[26–30] to longer-ranged Heisenberg[28,31] and Kitaev[32] interactions. Based on the extended exchange models with hopping terms, which are called the one-band t–J-like model, theoretical studies[33–35] have shown that a single hole moves incoherently at high energies and hidden quasiparticles arise at low energies in the zigzag magnetic phase. In these works, the hole has only one degree of freedom. However, in real materials, a hole doped in Ir^{4+} of Na_2IrO_3, i.e., removing an electron from t_{2g}^5 configuration, can be doped not only into $j = 1/2$ (single-electron state) states but also into $j = 3/2$ states. The multiple habitability of a hole makes the hole propagation more complicated than that in previous works.[33–35] Therefore, the dynamics of a single hole doped into the t_{2g}^5 states in the zigzag phase on the honeycomb lattice deserves further studies.

Experimentally, ARPES studies[36–39] have found various features in the low-energy electronic structure in Na_2IrO_3. Comin *et al.*[36] detected four flat bands and a clear insulating gap of ~ 340 meV, which is explained by the interference between the two sublattices of the honeycomb lattice.[33] Alidoust *et al.*[37] and Rodriguez *et al.*[39] reported the observation of metallic states at the center of the Brillouin zone. Moreschini *et al.*[38] found that the dispersion of the lowest-energy state near the Γ point is electron-like and does not cross the Fermi level, and that there exist flat bands at ~ 0.7 eV and dispersive hole-like states in the higher-energy region. The intensity of the flat bands focuses on the M point, and that of the hole-like states near ~ 1.2 eV is centered on the K point. The charge dynamics in Na_2IrO_3 revealed by these experiments are much more complex than the previous theoretical results based on the one-band t–J-like models.[33–35] Therefore, the understanding of the spectral characteristics unveiled by ARPESs in the spin-orbit assisted Mott insulator Na_2IrO_3 remains an open problem.

In this Letter, based on the multi-band t–J-like Hamil-

*Corresponding authors. Email: slyu@nju.edu.cn; jxli@nju.edu.cn
© 2023 Chinese Physical Society and IOP Publishing Ltd

tonian derived from the t_{2g} three-orbital Hubbard model in Na_2IrO_3, we investigate the dynamics of a single hole doped into the zigzag magnetic ordering state of Na_2IrO_3 with internal degrees of freedom (IDFs), using the self-consistent Born approximation (SCBA). The IDF of the doped hole means that it does not only form a singlet but also triplet and quintet states. According to the conservation of the total angular momentum J, we classify the t_{2g}^4 states, which are referred to as the IDF of the hole, into two singlet states, one triplet state, and two quintet states, as illustrated in Fig. 1(c). We find that the lowest-energy spectrum is dominated by the motion of the singlet $J=0$ hole and exhibits an electron-like dispersion (opening upward) near the Γ point. The mid-energy and high-energy spectra are attributed to the motion of the triplet $J=1$ and quintet $J=2$ holes, respectively. The weight of the mid-energy spectra is concentrated on the M point, consistent with the experiment observation.[38] The high-energy spectra exhibit a hole-like dispersion (opening downward) along the Γ–K path. The overall features of spectra are robust, even when Hund's coupling J_H is changed from 0.17 eV to 0.51 eV, and are qualitatively irrelevant to the exchange model. The interference between IDFs in different sublattices plays a significant role in inducing the complex dispersions.

In order to discuss the motion of a single hole in the magnetically ordered background, the t–J-like model is always used as the starting point[4,40] and could be derived from the multi-orbital Hubbard model by perturbation theory in the strong-coupling limit:[41,42]

$$H_{tJ} = P_0 \sum_{ipp'} \left(\epsilon_{ip}\delta_{pp'} + \Delta_i^{pp'}\right) X_i^{pp'} P_0 + P_0 \sum_{\substack{i<j \\ rr'ss'}} \left(V_{ij}^{rr',ss'} X_i^{rr'} X_j^{ss'} + \text{H.c.}\right) P_0 + H_{\text{ex}}, \quad (1)$$

where H_{ex} contains the exchange interactions between the $J=1/2$ pseudospins. P_0 projects Hilbert space into the low-energy states including the $J=1/2$ states of t_{2g}^5 configuration and the $J=0$, 1, 2 states of t_{2g}^4 manifold as shown in Fig. 1(c). $X_i^{pp'} = |ip\rangle\langle ip'|$, where $|ip\rangle$ satisfies $(H_i^U + H_i^\lambda)|ip\rangle = \epsilon_{ip}|ip\rangle$, is a Hubbard operator on the i-th site. $H_i^\lambda = \lambda \boldsymbol{l}_i \cdot \boldsymbol{s}_i$ is the electron-spin–orbit interaction. Here, H_i^U contains intra-orbital Coulomb interaction U, inter-orbital Coulomb interaction U', Hund's coupling J_H, and pairing hoping interaction J_P with $J_P = J_H$ and $U = U' + 2J_H$. $\Delta_i^{pp'} = \langle ip|H_i^\Delta|ip'\rangle$ is the matrix element of the crystal field. $V_{ij}^{rr',ss'} = \sum_{\nu\nu'} t_{ij}^{\nu\nu'} \langle ir, js|c_{i\nu}^\dagger c_{j\nu'}|ir', js'\rangle$, where $c_{j,\nu'\equiv(l,\sigma)}$ annihilates an electron with spin σ in the l-th orbital state at site j, are the parameters of hopping between the $J=1/2$ states and t_{2g}^4 states; $t_{ij}^{\nu\nu'}$ are the original hopping parameters between t_{2g} orbitals.

To investigate the motion of a hole, we introduce hole fermions $f_{is}^\dagger$ and Schwinger bosons $b_{is'}^\dagger$, which correspond to the t_{2g}^4 and $J=1/2$ states (see Fig. 1), respectively. Correspondingly, the electron operator in the low-energy space could be expressed by $c_{i\nu} = \sum_{ss'} \tilde{U}_{ss'}^{i\nu} f_{is}^\dagger b_{is'}$ with constraint $\sum_{s'} b_{is'}^\dagger b_{is'} + \sum_s f_{is}^\dagger f_{is} = 1$. Since the ground state of Na_2IrO_3 is long-range zigzag ordering, the low-energy spin excitations are well described by the magnons. Within the linear spin-wave approximation (LSW), one Schwinger boson b_{i0} is condensed and other bosons are mapped to Holstein–Primakoff bosons.[43,44] Using the Fourier transformation[45,46] $f_{\boldsymbol{k}\alpha s}^\dagger = \sqrt{4/N}\sum_m f_{m\alpha s}^\dagger e^{i\boldsymbol{k}\cdot\boldsymbol{r}_{m\alpha}}$, where N is the number of sites and (m,α) label the α-th sublattice in the m-th magnetic unit cell, we re-express the t–J-like model [Eq. (1)] in the matrix form within LSW as follows:

$$H_{fb} = \sum_{\boldsymbol{k}} \hat{f}_{\boldsymbol{k}}^\dagger \hat{h}(\boldsymbol{k}) \hat{f}_{\boldsymbol{k}} + \sum_{\boldsymbol{q},n} \omega_{n\boldsymbol{q}} \gamma_{n,\boldsymbol{q}}^\dagger \gamma_{n,\boldsymbol{q}} + \sum_{\boldsymbol{k}\boldsymbol{q}n} \hat{f}_{\boldsymbol{k}}^\dagger \left[\hat{g}_n(\boldsymbol{k},\boldsymbol{q})\gamma_{n,\boldsymbol{q}} + \hat{g}_n^\dagger(\boldsymbol{k}-\boldsymbol{q},-\boldsymbol{q})\gamma_{n,-\boldsymbol{q}}^\dagger\right] \hat{f}_{\boldsymbol{k}-\boldsymbol{q}}, \quad (2)$$

where $\omega_{n\boldsymbol{q}}$ is the dispersion of the magnons $\gamma_{n,\boldsymbol{q}}^\dagger$, $\hat{h}(\boldsymbol{k})$ is the Hamiltonian of the free hole, and $\hat{g}_n(\boldsymbol{k},\boldsymbol{q})$ describes the coupling between the t_{2g}^4 hole and the magnons. Here, $\hat{h}(\boldsymbol{k})$ and $\hat{g}_n(\boldsymbol{k},\boldsymbol{q})$ have a matrix form, and the detailed derivations are given in the Supplemental Materials.[42]

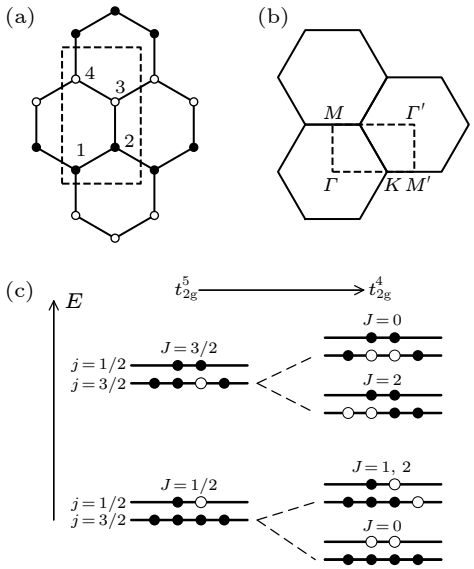

Fig. 1. (a) Magnetic structure of the zigzag ordering, where the filled and open sites denote up pseudospin and down pseudospin, respectively. The rectangle is magnetic unit cell. (b) Structure of the reciprocal space. M, Γ, K, M', and Γ' are the high-symmetry points. (c) States of t_{2g}^5 and t_{2g}^4 configurations in iridium ion. Filled and open circles stand for occupied and non-occupied electrons, respectively. J (j) is multi-particle (single-particle) total angular momentum, respectively. The circles from left to right on each line represent $|m=-j,\ldots,j\rangle$ states, respectively.

As the spectral properties measured in ARPES experiments are related to single-particle Green's function, we introduce two relevant Green's functions $\hat{G}^d(\boldsymbol{k},\omega) = \langle 0|\hat{d}_{\boldsymbol{k}}(\omega+i\eta-H_{fb})^{-1}\hat{d}_{\boldsymbol{k}}^\dagger|0\rangle$, where $|0\rangle$ is the ground state of the exchange term H_{ex} under the LSW and $d = f(c^\dagger)$ corresponds to the hole (physical) Green function $\hat{G}^{f/c}(\boldsymbol{k},\omega)$, respectively. The hole Green function is determined by the self-consistent equation under the SCBA.[4] The electron operator $c_{\boldsymbol{k}\nu} = \sqrt{4/N}\sum_i c_{i\nu} e^{i\boldsymbol{k}\cdot\boldsymbol{r}_i}$ in the low-energy

space could be expressed by hole operators and magnon operators

$$c_{\boldsymbol{k}\nu} = \hat{f}^{\dagger}_{\boldsymbol{k}}\hat{W}^{\nu}(\boldsymbol{k}) + \sum_{\boldsymbol{q}n}\hat{f}^{\dagger}_{\boldsymbol{k}-\boldsymbol{q}}[\hat{Y}^{\nu}_{n}(\boldsymbol{k},\boldsymbol{q})\gamma^{\dagger}_{n,\boldsymbol{q}} + \hat{Y}^{\prime\nu}_{n}(\boldsymbol{k},-\boldsymbol{q})\gamma_{n,-\boldsymbol{q}}], \quad (3)$$

where $\hat{W}^{\nu}$ [42] describes the creation amplitude of a single hole by moving an electron from zigzag state and $\hat{Y}^{\nu}_{n}$ ($\hat{Y}^{\prime\nu}_{n}$) [42] denotes the creation (annihilation) amplitude of a magnon plus a single hole. Base on this, the physical Green function can be calculated with Eq. (S20) in the Supplemental Materials. [42] The corresponding spectral functions for two Green's functions are defined as $A^{f}_{s}(\boldsymbol{k},\omega) = -\frac{1}{\pi}\mathrm{Im}\sum_{\alpha\beta}G^{f}_{\alpha s,\beta s}(\boldsymbol{k},\omega)$ and $A^{c}(\boldsymbol{k},\omega) = -\frac{1}{\pi}\mathrm{Tr}[\mathrm{Im}\hat{G}^{c}(\boldsymbol{k},\omega)]$. In the following calculations, we choose 16×8 magnetic unit cells [Fig. 1(a)] and employ $U = 1.7\,\mathrm{eV}$, $J_{\mathrm{H}} = 0.3\,\mathrm{eV}$, and $\lambda = 0.4\,\mathrm{eV}$, [28] unless otherwise specified. For the classical ground state of the exchange term H_{ex}, we assume it is a zigzag order. The hopping parameters $t^{\nu\nu'}_{ij}$ and the crystal field H^{Δ}_{i} are taken from Ref. [28]. The IDF are only considered up to the nine low-energy states, i.e., $J = 0$, 1, 2 states [Fig. 1(c)].

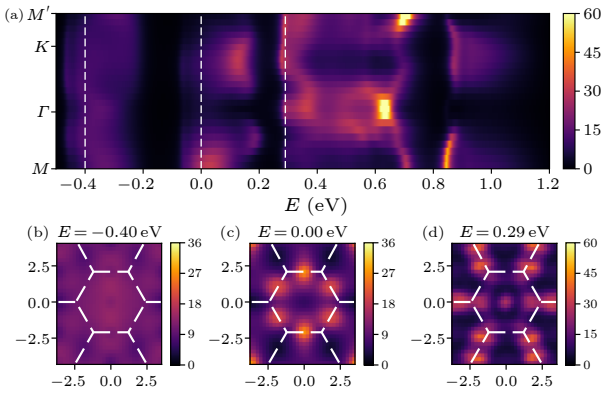

Fig. 2. (a) Physical spectral function $A^{c}(\boldsymbol{k},\omega)$ along the high-symmetry path M–Γ–K–M' as indicated in Fig. 1(b). The dashed lines denote the constant-energy cuts at $-0.40\,\mathrm{eV}$, $0.00\,\mathrm{eV}$, and $0.29\,\mathrm{eV}$ as plotted in (b), (c), and (d) respectively. (b)–(d) Constant-energy contour maps of $A^{c}(\boldsymbol{k},\omega)$. The thick dashed lines denote Brillouin zone boundaries.

Let us first discuss the physical spectral function $A^{c}(\boldsymbol{k},\omega)$ which directly relates to the ARPES results, as shown in Fig. 2. Figure 2(a) shows that the low-energy spectrum (around $-0.4\,\mathrm{eV}$) has an electron-like dispersion near the Γ point, which is well consistent with ARPES experiments. [37,38] The corresponding contour map in Fig. 2(b) exhibits maximum intensity near the Γ point. In the mid-energy region between $-0.1\,\mathrm{eV}$ and $0.2\,\mathrm{eV}$, the spectrum along the Γ–K path hosts a downward parabolic dispersion and the intensities near the Γ point are suppressed heavily. From the energy cut in Fig. 2(c), we can see that the intensities of spectrum are concentrated around the M point, which is consistent with the features of the 0.7-eV flat band in ARPES experiment. [38] In the high-energy region between $0.4\,\mathrm{eV}$ and $0.6\,\mathrm{eV}$, the intensities between Γ point and K point are suppressed and a hole-like dispersion arises along the Γ–K direction. Furthermore, the maximum intensities of spectrum at $0.29\,\mathrm{eV}$ are shifted from near the M point to near the K point, relative to the the maximum intensities at $0.0\,\mathrm{eV}$, as shown in Fig. 2(d). These features are also in agreement with experiment. [38] In addition, our investigations have shown a similarity between the low-energy spectrum observed at the Γ point and the entirety of the Γ-point spectrum documented in earlier studies, [33–35] where the incoherent high-energy spectral weight at the Γ point aligns with the spectral weight near $-0.3\,\mathrm{eV}$ in our study. However, it is worth highlighting that the intermediate- and high-energy spectra exhibit distinct characteristics that deviate from those observed in previous investigations based on the one-band t–J-like model. [33–35]

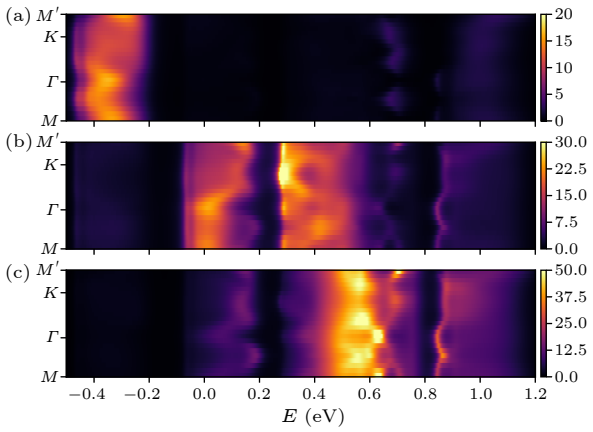

Fig. 3. Spectral function $A^{f}_{s}(\boldsymbol{k},\omega)$ of a hole with IDF along the high-symmetry path M–Γ–K–M' as indicated in Fig. 1(b). (a) Spectral function $A^{f}_{0}(\boldsymbol{k},\omega)$ of the $J = 0$ hole. (b) Spectral function $A^{f,1}(\boldsymbol{k},\omega)$ of the $J = 1$ hole. (c) Spectral function $A^{f,2}(\boldsymbol{k},\omega)$ of the $J = 2$ hole.

To understand the contribution of the hole with different IDF to the physical spectral function, we turn to the hole spectral function $A^{f}_{s}(\boldsymbol{k},\omega)$ with different total angular momenta. Figure 3(a) shows the spectral function $A^{f}_{0}(\boldsymbol{k},\omega)$ of the hole with total angular momentum $J = 0$. The spectral intensities of $A^{f}_{0}(\boldsymbol{k},\omega)$ are mainly concentrated in the low-energy region. This suggests that the low-energy spectra in $A^{c}(\boldsymbol{k},\omega)$ come basically from the motion of the singlet $J = 0$ hole. Figure 3(b) shows the spectral function $A^{f,1}(\boldsymbol{k},\omega) = \sum_{s=-1}^{1}A^{f}_{s}(\boldsymbol{k},\omega)$ of the triplet $J = 1$ hole. The weights of the triplet-hole spectra are concentrated in the mid-energy region, indicating that the mid-energy spectra in $A^{c}(\boldsymbol{k},\omega)$ (see Fig. 2) are dominated by the motion of the triplet $J = 1$ hole, although there is also a contribution from the motion of the $J = 2$ hole as shown in Fig. 3(c), where the spectral function $A^{f,2}(\boldsymbol{k},\omega) = \sum_{s=-2}^{2}A^{f}_{s}(\boldsymbol{k},\omega)$ of the quintet $J = 2$ hole is exhibited. From the mid-energy spectra in Figs. 3(b) and 3(c), we find that the intensities near the Γ point are not suppressed, on contrary to the spectra in the physical spectral function $A^{c}(\boldsymbol{k},\omega)$ of Fig. 2. This is due to the absence of the vertex $\hat{W}$ that would give rise to the interference between IDFs in different sublattices.

To gain more insights into the scattering process, we present the physical spectral functions induced by the

nearly free hole (by setting the coupling $\hat{g}_n(\boldsymbol{k},\boldsymbol{q}) = 0$) and only-scattered hole (by setting $\hat{h}(\boldsymbol{k}) = 0$ except the on-site terms) in Figs. 4(a) and 4(b), respectively. Figure 4(a) shows that the dispersion of the lowest-energy band near the Γ point is electron-like, and a near flat band with strongly M-point intensity appears in the mid-energy region around 0.02 eV. From Fig. 4(b), it is clearly seen that the spectrum takes the shape of a ladder. This feature implies that the hole moving in the zigzag order background is strongly scattered by the magnons, which is similar to the string excitation in a Néel spin background.[40] Compared with Fig. 4(a), the bands in Fig. 2(a) are greatly broadened and heavily renormalized, but the main features, including electron-like dispersion near the Γ point and high M-point intensity of mid-energy states, remain.

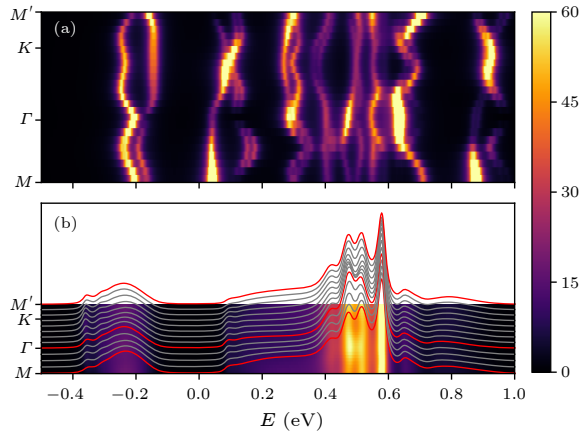

Fig. 4. Physical spectral functions $A^c(\boldsymbol{k},\omega)$ for (a) the nearly free hole and (b) the only-scattered hole (see text).

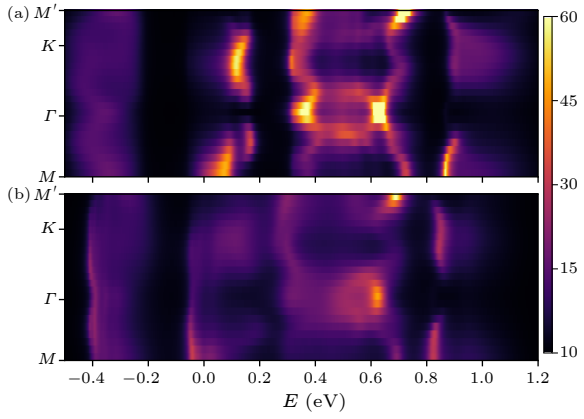

Fig. 5. Physical spectral function $A^c(\boldsymbol{k},\omega)$ for Hund's coupling $J_{\rm H} = 0.17$ eV (a) and 0.51 eV (b).

It is noteworthy that the main features mentioned above remain robust even when Hund's coupling $J_{\rm H}$ is altered, as depicted in Figs. 5(a) and 5(b), where $J_{\rm H}$ is changed from 0.3 eV to 0.17 eV and 0.51 eV, respectively. As $J_{\rm H}$ increases, the gap between the singlet and triplet hole (near -0.2 eV) decreases, and both the low-energy dispersion near the Γ point and the mid-energy dispersion near the M point become flatter [Fig. 5(b)]. The reduction of the gap is mainly due to the decreasing difference of the on-site energy between the singlet and triplet states of the hole, as $J_{\rm H}$ increase, i.e., $\epsilon_{J=1}-\epsilon_{J=0} = (\sqrt{25J_{\rm H}^2 + 10\lambda J_{\rm H} + 9\lambda^2} - 5J_{\rm H})/2$. In the mid-energy region, the increase of $J_{\rm H}$ causes the spectra shown in Fig. 5(b) to extend further, resulting in a reduction of the gap Δ_1 (near 0.2 eV). The hole-like dispersion along the Γ–K path at high-energy region still remains with the increase of $J_{\rm H}$. Moreover, these overall features are also observed[42] when we replace the exchange term $H_{\rm ex}$ in Eq. (1) with the exchange model obtained from the exact diagonalization method.[28]

Based on the physical and hole spectral function, we suggest that the ARPES spectra at low, medium, and high energies are predominantly influenced by the singlet, triplet, and quintet states, respectively. Our findings qualitatively reproduce the key characteristics of the ARPES spectra, including (i) an electron-like dispersion near the Γ point at low energies, (ii) a flat band with spectral weights concentrated on the M point, and (iii) a high-energy hole-like dispersion along the Γ–K path. These agreements with experimental observations suggest that Na_2IrO_3 is a spin-orbit Mott insulator. Quantitatively, the energy gap near -0.2 eV and the gap Δ_1 are not clearly observed in ARPES experiments.[36–39] The low-energy spectrum, instead of being concentrated near the Γ point as expected, disperses throughout the Brillouin zone. This is inconsistent with the experimental findings.[37–39] This inconsistency may arise from neglecting the matrix-element effect and the mixing between $j = 1/2$ and $3/2$ states. Additionally, the high-energy spectra above 0.7 eV also deviate from the ARPES results due to the neglect of the high-energy IDF, as illustrated in Fig. 1(c). In contrast to previous theoretical works on Na_2IrO_3,[33–35] our study takes into account more IDFs of the hole. In the previous works, the hole corresponds to the missing $J = 1/2$ state, which is associated only with the singlet state in our current research. In contrast to the similar study on Sr_2IrO_4,[47] we find that in Na_2IrO_3, the spectra from the quintet and triplet states overlap heavily, and the interference between IDFs in different sublattices plays a significant role in producing the dispersion at medium and high energies.

In summary, we have studied the dynamics of a hole with IDFs under the zigzag magnetic background in Na_2IrO_3 and explain various features in the ARPES spectra using the SCBA. We find that the electron-like dispersive states in the low-energy region arise from the singlet hole, while the flat band with maximum M-point intensities in the mid-energy region is attributed to the motion of the triplet hole. The hole-like dispersive spectra in the high-energy region are due to the motion of the quintet hole. The interference between IDFs of hole in different sublattices plays a significant role in producing the complex dispersions. However, to accurately reproduce the fine structure of the ARPES spectra, additional information such as the matrix-element effects and the mixing between the $j = 1/2$ and $3/2$ states may need to be considered.

Acknowledgements. This work was supported by the National Key Projects for Research and Development of China (Grant No. 2021YFA1400400), the National Natural Science Foundation of China (Grant Nos. 12004191, 92165205, and 12074175), the Natural Science Founda-

tion of Jiangsu Province (Grant No. BK20200738), and the Natural Science Research Start-up Foundation of Posts and Telecommunications (Grant No. NY220095).

References

[1] Lee P A, Nagaosa N, and Wen X G 2006 *Rev. Mod. Phys.* **78** 17
[2] Liang S, Doucot B, and Anderson P W 1988 *Phys. Rev. Lett.* **61** 365
[3] Zhang F C and Rice T M 1988 *Phys. Rev. B* **37** 3759
[4] Kane C L, Lee P A, and Read N 1989 *Phys. Rev. B* **39** 6880
[5] Martinez G and Horsch P 1991 *Phys. Rev. B* **44** 317
[6] Liu Z P and Manousakis E 1991 *Phys. Rev. B* **44** 2414
[7] Dagotto E 1994 *Rev. Mod. Phys.* **66** 763
[8] Leung P W and Gooding R J 1995 *Phys. Rev. B* **52** R15711
[9] Damascelli A, Hussain Z, and Shen Z X 2003 *Rev. Mod. Phys.* **75** 473
[10] Kim B J, Jin H, Moon S J, Kim J Y, Park B G, Leem C S, Yu J, Noh T W, Kim C, Oh S J, Park J H, Durairaj V, Cao G, and Rotenberg E 2008 *Phys. Rev. Lett.* **101** 076402
[11] Kim B J, Ohsumi H, Komesu T, Sakai S, Morita T, Takagi H, and Arima T 2009 *Science* **323** 1329
[12] Singh Y and Gegenwart P 2010 *Phys. Rev. B* **82** 064412
[13] Singh Y, Manni S, Reuther J, Berlijn T, Thomale R, Ku W, Trebst S, and Gegenwart P 2012 *Phys. Rev. Lett.* **108** 127203
[14] Rau J G, Lee E K H, and Kee H Y 2016 *Annu. Rev. Condens. Matter Phys.* **7** 195
[15] Jackeli G and Khaliullin G 2009 *Phys. Rev. Lett.* **102** 017205
[16] Kim B H, Shirakawa T, and Yunoki S 2016 *Phys. Rev. Lett.* **117** 187201
[17] Plumb K W, Clancy J P, Sandilands L J, Shankar V V, Hu Y F, Burch K S, Kee H Y, and Kim Y J 2014 *Phys. Rev. B* **90** 041112
[18] Banerjee A, Bridges C A, Yan J Q, Aczel A A, Li L, Stone M B, Granroth G E, Lumsden M D, Yiu Y, Knolle J, Bhattacharjee S, Kovrizhin D L, Moessner R, Tennant D A, Mandrus D G, and Nagler S E 2016 *Nat. Mater.* **15** 733
[19] Winter S M, Tsirlin A A, Daghofer M, van den Brink J, Singh Y, Gegenwart P, and Valentí R 2017 *J. Phys.: Condens. Matter* **29** 493002
[20] Ran K J, Wang J H, Wang W, Dong Z Y, Ren X, Bao S, Li S C, Ma Z, Gan Y, Zhang Y T, Park J T, Deng G, Danilkin S, Yu S L, Li J X, and Wen J 2017 *Phys. Rev. Lett.* **118** 107203
[21] Kitaev A 2006 *Ann. Phys.* **321** 2
[22] Johnson R D, Williams S C, Haghighirad A A, Singleton J, Zapf V, Manuel P, Mazin I I, Li Y, Jeschke H O, Valentí R, and Coldea R 2015 *Phys. Rev. B* **92** 235119
[23] Cao H B, Banerjee A, Yan J Q, Bridges C A, Lumsden M D, Mandrus D G, Tennant D A, Chakoumakos B C, and Nagler S E 2016 *Phys. Rev. B* **93** 134423
[24] Chaloupka J, Jackeli G, and Khaliullin G 2010 *Phys. Rev. Lett.* **105** 027204
[25] Chaloupka J, Jackeli G, and Khaliullin G 2013 *Phys. Rev. Lett.* **110** 097204
[26] Rau J G, Lee E K H, and Kee H Y 2014 *Phys. Rev. Lett.* **112** 077204
[27] Yamaji Y, Nomura Y, Kurita M, Arita R, and Imada M 2014 *Phys. Rev. Lett.* **113** 107201
[28] Winter S M, Li Y, Jeschke H O, and Valentí R 2016 *Phys. Rev. B* **93** 214431
[29] Kim H S and Kee H Y 2016 *Phys. Rev. B* **93** 155143
[30] Wang W, Dong Z Y, Yu S L, and Li J X 2017 *Phys. Rev. B* **96** 115103
[31] Kimchi I and You Y Z 2011 *Phys. Rev. B* **84** 180407
[32] Rousochatzakis I, Reuther J, Thomale R, Rachel S, and Perkins N B 2015 *Phys. Rev. X* **5** 041035
[33] Trousselet F, Berciu M, Oleś A M, and Horsch P 2013 *Phys. Rev. Lett.* **111** 037205
[34] Trousselet F, Horsch P, Oleś A M, and You W L 2014 *Phys. Rev. B* **90** 024404
[35] Wang B B, Wang W, Yu S L, and Li J X 2018 *J. Phys.: Condens. Matter* **30** 385602
[36] Comin R, Levy G, Ludbrook B, Zhu Z H, Veenstra C N, Rosen J A, Singh Y, Gegenwart P, Stricker D, Hancock J N, van der Marel D, Elfimov I S, and Damascelli A 2012 *Phys. Rev. Lett.* **109** 266406
[37] Alidoust N, Liu C, Xu S Y, Belopolski I, Qi T, Zeng M, Sanchez D S, Zheng H, Bian G, Neupane M, Liu Y T, Wilson S D, Lin H, Bansil A, Cao G, and Hasan M Z 2016 *Phys. Rev. B* **93** 245132
[38] Moreschini L, Lo V I, Breznay N P, Moser S, Ulstrup S, Koch R, Wirjo J, Jozwiak C, Kim K S, Rotenberg E, Bostwick A, Analytis J G, and Lanzara A 2017 *Phys. Rev. B* **96** 161116
[39] Rodriguez J, Lopez G, Ramirez F, Breznay N P, Kealhofer R, Nagarajan V, Latzke D, Wilson S, Marrufo N, Santiago P, Lara J, Diego A, Molina E, Rosser D, Tavassol H, Lanzara A, Analytis J G, and Ojeda-Aristizabal C 2020 *Phys. Rev. B* **101** 235415
[40] Liu Z P and Manousakis E 1992 *Phys. Rev. B* **45** 2425
[41] Yin W G and Ku W 2009 *Phys. Rev. B* **79** 214512
[42] See Supplemental Materials for the detail derivation, and the spectra with different models.
[43] Muniz R A, Kato Y, and Batista C D 2014 *Prog. Theor. Exp. Phys.* **2014** 83I01
[44] Dong Z Y, Wang W, and Li J X 2018 *Phys. Rev. B* **97** 205106
[45] Lüscher A, Läuchli A, Zheng W, and Sushkov O P 2006 *Phys. Rev. B* **73** 155118
[46] Sushkov O P, Sawatzky G A, Eder R, and Eskes H 1997 *Phys. Rev. B* **56** 11769
[47] Pärschke E M, Wohlfeld K, Foyevtsova K, and van den Brink J 2017 *Nat. Commun.* **8** 686